Search for light sterile neutrinos from $W^{\pm}$ decays at the LHC

Claudio O. Dib[1,†], C. S. Kim[2,3,*], and Sebastian Tapia Araya[4,‡]

[1]*Department of Physics and CCTVal, Universidad Técnica Federico Santa María, Valparaíso 2340000, Chile*
[2]*Department of Physics and IPAP, Yonsei University, Seoul 120-749, Korea*
[3]*Institute of High Energy Physics, Dongshin University, Naju 58245, Korea*
[4]*Department of Physics, University of Illinois at Urbana-Champaign, Urbana, Illinois 61801, USA*

We study the feasibility to observe sterile neutrinos with masses in the range 5 GeV $< m_N <$ 20 GeV at the LHC, using exclusive semileptonic modes involving pions, $W \to \ell N \to \pi\ell\ell$, $2\pi\ell\ell$, and $3\pi\ell\ell$. We thus cover a mass window that is between what can be studied in meson factories and high-energy colliders. We run simulations for these exclusive events, where pions should be distinguished from the background provided the neutrino decay exhibits a vertex displacement from its production point. In a previous work, we have estimated the theoretical rates, and here we analyze the observability of the processes at the LHC, given the fact that exclusive hadronic states may be difficult to identify. We study the sensitivity bounds for the observation and discovery of sterile neutrinos in the above mass range. By the end of run 3, current bounds on heavy-to-light lepton mixings in the lower-mass end ($\sim$5 GeV) could be improved by about an order of magnitude to $|U_{\ell N}|^2 \sim 5 \times 10^{-6}$, and the High-Luminosity LHC could reach $|U_{\ell N}|^2 \lesssim 3 \times 10^{-7}$ in the mass range below 11 GeV. Studying in addition equal-sign and opposite-sign dileptons, the Majorana or Dirac character of the sterile neutrino could be revealed.

I. INTRODUCTION

The discovery of neutrino oscillations [1–3] implies that at least two of the three neutrinos that participate in the weak interactions must be massive. Since neutrinos are massless in the Standard Model, these particles have become an important portal to physics beyond the Standard Model [4–7]. Now, the smallness of the observed neutrino masses is usually explained by introducing right-handed neutrinos, which must be sterile under electroweak interactions, inducing scenarios with a seesaw mechanism [8–14]. While originally the seesaw mechanism resorted to the presence of very heavy extra neutrinos, there are also models where the extra fields are not so heavy, leaving the open possibility that the extra sterile neutrinos could have masses in the broad range from eV to TeV [15], and so experimental searches must also cover all those possibilities. Indeed, there are plenty of scenarios in the literature to explain the light neutrino masses. These masses can be generated at tree level or as loop contributions, and they almost invariably require the inclusion of extra fields. The so-called types I, II, and III include fermion singlets, scalar triplets, and fermion triplets, respectively. Loop-generated masses also include extra fields, typically scalars and/or fermions. Some of the scenarios may contain candidates for dark matter. In summary, in order to discriminate from the different scenarios that extend the Standard Model (SM), it will be important to know at least whether there exist extra neutral fermions and, in the affirmative case, to know their masses and whether they are Majorana or Dirac particles.

LHC searches for sterile neutrinos with a mass above 100 GeV [16,17] are based on the inclusive processes $pp \to W^*X$, $W^* \to \ell^{\pm}\ell^{\pm}jj$ [18–21]. For m_N below M_W, the jets are not energetic enough to pass the background reduction cuts, so purely leptonic modes $W^{(*)} \to \ell\ell\ell\nu$ could be preferred [22–28], even though they have the problem of missing energy and the flavor number due to the undetectable final neutrino. However, as one goes to lower m_N searches, again low-p_t leptons plus missing neutrinos affect the observability of these leptonic decays. Now, for neutrino masses below 20 GeV, there is an advantage: The neutrino may live long enough to leave an observable displacement from its production to its decay point [29–38], a feature that helps drastically reduce the

[*]Corresponding author.
cskim@yonsei.ac.kr
[†]claudio.dib@usm.cl
[‡]s.tapia@cern.ch

backgrounds. We then proposed to go back to using semileptonic modes for the searches in this mass range but now with exclusive channels instead of jets [39]. Again, for m_N below 5 GeV, B factories may be more appropriate to search for the sterile neutrino than high-energy hadron colliders, due to the cleaner environment and the production of N in B or lighter meson decays [40–44].

For the sterile neutrino mass range of 5 GeV $< m_N <$ 20 GeV, in a previous work [39] we proposed to use neither $\ell\ell jj$ nor trilepton events but the exclusive semileptonic processes $W \to \mu N$, followed by $N \to \mu\pi$, $\mu\pi\pi$, and $\mu\pi\pi\pi$, which are modes with no missing energy. The decay channels $N \to e\pi, e\pi\pi, e\pi\pi\pi$ in the secondary process were not considered in order to avoid misidentification of electrons and pions. We concluded that the most promising modes should be $W^+ \to \mu^+ N$ followed by a displaced decay, either $N \to \pi\mu^+$, $2\pi\mu^+$, or $3\pi\mu^+$ for a Majorana sterile neutrino or $W^+ \to \mu^+ N$ followed by $N \to \pi\mu^-$, $2\pi\mu^-$, or $3\pi\mu^-$ for a Dirac neutrino. We studied those rates, including the comparison of different models for the pion form factors.

Now in this article we want to complement the previous work by studying the observability of these processes at the LHC. In general, the observability of these modes is not a trivial matter, since pions with relatively low p_T need to be selected from backgrounds; neutral pions, which decay almost instantly into $\gamma\gamma$, are also difficult to identify; pions and electrons should be clearly distinguished in order to avoid fake signals. On the other hand, the vertex separation due to the sizable lifetime of the sterile neutrino with a mass below 20 GeV [29–38] can help reject considerably all backgrounds.

In Sec. II, we review the processes in question in a very brief form, as more details can be found in a previous work [39]. In Sec. III, we present our current analysis and simulations, where we study the detectability of the processes at the LHC. In Sec. IV, we state our conclusions.

II. THEORETICAL SUMMARY OF THE PROCESSES

Here, we give a short summary on our previous work on the decay $W \to \ell N$ and decays $N \to \ell n\pi$ with $n = 1, 2, 3$. Detailed formulas with full theoretical discussions are shown in Ref. [39].

A. The decay $W \to \ell N$

The leptonic sector in a generic SM extension includes one or more extra neutral lepton singlets N, in addition to the three generations of left-handed SM $SU(2)_L$ lepton doublets. The neutral lepton singlets N are *sterile*, in the sense that they do not directly interact with other SM particles except through mixing with the active neutrinos.

At the LHC, sterile neutrinos with masses around 5–20 GeV will be mainly produced from the decay of on-shell W bosons. The decay rate $W^+ \to \ell^+ N$ can be easily calculated; neglecting the charged lepton mass, the branching ratio is

$$
\begin{aligned}
\mathcal{B}(&W^+ \to \ell^+ N) \\
&\equiv \frac{\Gamma(W^+ \to \ell^+ N)}{\Gamma_W} \\
&= \frac{G_F}{\sqrt{2}} \frac{M_W^3}{12\pi\Gamma_W} |U_{\ell N}|^2 \left(2 + \frac{m_N^2}{M_W^2}\right)\left(1 - \frac{m_N^2}{M_W^2}\right)^2,
\end{aligned} \quad (1)
$$

where $\Gamma_W \simeq 2.085$ GeV is the total decay width of the W boson [45]. From here, the neutrino N can decay in several modes, depending on its mass. Here, we are interested in the decays into pions, namely, $N \to \pi^\mp \ell^\pm$, $N \to \pi^0\pi^\mp\ell^\pm$, and $N \to \pi^\mp\pi^\mp\pi^\pm\ell^\pm$. Both charged modes will occur for a Majorana N, while for a Dirac N only the N decays into a negative charged lepton will be produced.

B. The decay $N \to \pi^- \ell^+$

The mode $N \to \pi^\mp\ell^\pm$ is a charged current process:

$$
\begin{aligned}
\Gamma(&N \to \pi^\mp\ell^\pm) \\
&= \frac{G_F^2}{16\pi} f_\pi^2 |V_{ud}|^2 |U_{\ell N}|^2 m_N^3 \lambda^{1/2}(1, m_\ell^2/m_N^2, m_{\pi^-}^2/m_N^2) \\
&\quad \times \left[\left(1 + \frac{m_\ell^2}{m_N^2} - \frac{m_\pi^2}{m_N^2}\right)\left(1 + \frac{m_\ell^2}{m_N^2}\right) - 4\frac{m_\ell^2}{m_N^2}\right],
\end{aligned} \quad (2)
$$

where m_π and m_N denote the mass of the charged pion and sterile neutrino, respectively; V_{ud} is the Cabibbo-Kobayashi-Maskawa matrix, and f_π is the pion decay constant; the function $\lambda(x, y, z)$ is defined as $\lambda(x, y, z) = x^2 + y^2 + z^2 - 2(xy + yz + zx)$. The formation of a single pion in the final state is relatively suppressed with respect to multipion modes, because it requires the two produced quarks to remain close together. Indeed, the suppression relative to the open quark production is about $\sim 4\pi^2 f_\pi^2/m_N^2$, which is $\sim 0.6\%$ for $m_N = 10$ GeV [39].

C. The decay $N \to \pi^0\pi^-\ell^+$

The decay into two pions, $N \to \pi^0\pi^-\ell^+$, is similar to the τ lepton decay $\tau^- \to \pi^0\pi^-\nu_\tau$ in terms of their interaction Lagrangian and Feynman diagram, except for the lepton flavor and charge. However, one must be aware that the kinematic range for the form factor in the N decays is extended to higher q^2, so an extrapolation of the τ form factor will be required. Considering the above, the differential decay rate for $N \to \pi^0\pi^-\ell^+$ can be written as

$$\frac{d\Gamma(N \to \pi^0\pi^-\ell^+)}{ds} = \frac{\Gamma_N^0|V_{ud}|^2|U_{\ell N}|^2}{2m_N^2} \frac{3s^3\beta_\ell\beta_\pi}{2m_N^6} F_-(s)^2$$
$$\times \left[\beta_\ell^2\left(\frac{(\Delta m_\pi^2)^2}{s^2} - \frac{\beta_\pi^2}{3}\right) + \left(\frac{(m_N^2 - m_\ell^2)^2}{s^2} - 1\right)\left(\frac{(\Delta m_\pi^2)^2}{s^2} + \beta_\pi^2\right)\right], \quad (3)$$

where $\Gamma_N^0 = G_F^2 m_N^5/(192\pi^3)$, $s = (p_{\pi^0} + p_{\pi^+})^2$, $\Delta m_\pi^2 \equiv m_{\pi^+}^2 - m_{\pi^0}^2$, $\beta_\ell = \lambda^{1/2}(1, m_\ell^2/s, m_N^2/s)$, $\beta_\pi = \lambda^{1/2}(1, m_{\pi^+}^2/s, m_{\pi^0}^2/s)$, and $F_-(s)$ is the hadronic form factor of the charged current, defined by

$$\langle\pi^-(p)\pi^0(p')|\bar{d}\gamma_\mu u|0\rangle = \sqrt{2}F_-(s)(p - p')_\mu. \quad (4)$$

The decay rate is then obtained after integrating over s, within the limits $s_- = (m_{\pi^-} + m_{\pi^0})^2$ and $s_+ = (m_N - m_\ell)^2$. This expression is analogous to $\Gamma(\tau^- \to \pi^0\pi^-\nu_\tau)$ [46,47]. The form factor $F_-(s)$ in the timelike region, i.e., $s > 0$, is experimentally known from $\tau^- \to \pi^-\pi^0\nu_\tau$ [48] in the limited range $2m_\pi < \sqrt{s} < m_\tau$. The extrapolation to larger values of s is done in our previous work [39], based on two

alternatives: a vector dominance model [49] and on light front holographic QCD [50]. They both give very similar results [39].

D. The decay $N \to \pi^-\pi^-\pi^+\ell^+$

In much the same way as in the two-pion mode, the differential decay rate of the general hadronic decay $N \to h_1h_2h_3\ell^+$ can be written in terms of form factors with an expression identical to that of the τ decay $\tau^- \to h_1h_2h_3\nu_\tau$ [51], again provided that the form factors are extrapolated to larger values of q^2. Denoting the momentum and mass of the hadron h_i ($i = 1, 2, 3$) by p_i and m_i, respectively, and defining the momentum of the hadronic part by $q^\mu = (p_1 + p_2 + p_3)^\mu$, the differential decay rate can be expressed as

$$\frac{d\Gamma(N \to h_1h_2h_3\ell^+)}{dq^2} = \frac{G_F^2|V_{ud}|^2|U_{\ell N}|^2}{128(2\pi)^5 m_N^3}\lambda^{1/2}(1, m_N^2/q^2, m_\ell^2/q^2)\left[\left(\frac{(m_N^2 - m_\ell^2)^2}{q^2} - m_N^2 - m_\ell^2\right)\omega_{SA}(q^2)\right.$$
$$\left.+ \frac{1}{3}\left(\frac{(m_N^2 - m_\ell^2)^2}{q^2} + m_N^2 + m_\ell^2 - 2q^2\right)(\omega_A(q^2) + \omega_B(q^2))\right]. \quad (5)$$

In this expression, the functions $\omega_A(q^2)$, $\omega_B(q^2)$, and $\omega_{SA}(q^2)$ are given in Ref. [39].

The decay rate is obtained after integration over q^2 within the limits $q_-^2 = (m_1 + m_2 + m_3)^2$ and $q_+^2 = (m_N - m_\ell)^2$.

E. Theoretical results

With the expressions described above, we were able to estimate the exclusive semileptonic decay rates of N into $\pi\ell$, $2\pi\ell$, and $3\pi\ell$, for a neutrino N with a mass in the range 5–20 GeV, produced at the LHC in the process $W \to \ell N$. In Fig. 1 (left), we reproduce what we called the "canonical" decay rates for the modes $N \to n\pi + \ell^+$ and the inclusive estimate given by $N \to \bar{u}d\ell^+$ as a function of the neutrino mass m_N (canonical here means that all lepton-mixing elements $|U_{\ell N}|$ are factorized out of the expressions). In Fig. 1 (right), we show the canonical branching ratios for the full processes $W^+ \to N\ell^+ \to n\pi + \ell^+\ell^+$ and $W^+ \to N\ell^+ \to \bar{u}d\ell^+\ell^+$. The actual rates (left) and branching ratios (right) can be obtained by multiplying these canonical values by $|U_{\ell N}|^2$ (left) and $|U_{\ell N}|^4/\sum_{l'}|U_{\ell'N}|^2$ (right), respectively. From these figures, we were able to estimate the expected number of $W \to N\ell \to n\pi + \ell\ell$ events at the LHC, or, equivalently, the minimal value of

the lepton-mixing element that would generate five events or more, for a benchmark value of $m_N = 10$ GeV. At this mass, the figure gives a canonical branching ratio

$$\mathcal{B}(W^+ \to \pi^-\mu^+\mu^+, \pi^0\pi^-\mu^+\mu^+, \pi^+\pi^-\pi^-\mu^+\mu^+, \pi^0\pi^0\pi^-\mu^+\mu^+)$$
$$\equiv \mathcal{B}(W^+ \to n\pi + \mu^+\mu^+) \approx 8 \times 10^{-4}. \quad (6)$$

According to Ref. [52], at the end of the LHC run 2, one may expect a sample of $\mathcal{N}_W \sim 10^9$ W decays. Therefore, in order to obtain more than five events, we must have

$$\mathcal{N}_W \times \mathcal{B}(W^+ \to n\pi + \mu^+\mu^+) \times \frac{|U_{\mu N}|^4}{\sum_\ell|U_{\ell N}|^2} > 5,$$

which implies $|U_{\mu N}|^2 \gtrsim 6.2 \times 10^{-6}$, provided other mixing elements are smaller. If, instead, all mixing elements are comparable, then this lower bound increases by a factor of 3, i.e., $|U_{eN}|^2, |U_{\mu N}|^2, |U_{\tau N}|^2 \gtrsim 1.9 \times 10^{-5}$. These results are in ideal conditions, with no cuts or backgrounds. These bounds can be made about one order of magnitude stronger if one adds both charges and all lepton flavors $W^\pm \to n\pi + \ell^\pm\ell'^\pm$ ($n = 1, 2, 3$), i.e., $|U_{eN}|^2, |U_{\mu N}|^2, |U_{\tau N}|^2 \gtrsim 2 \times 10^{-6}$.
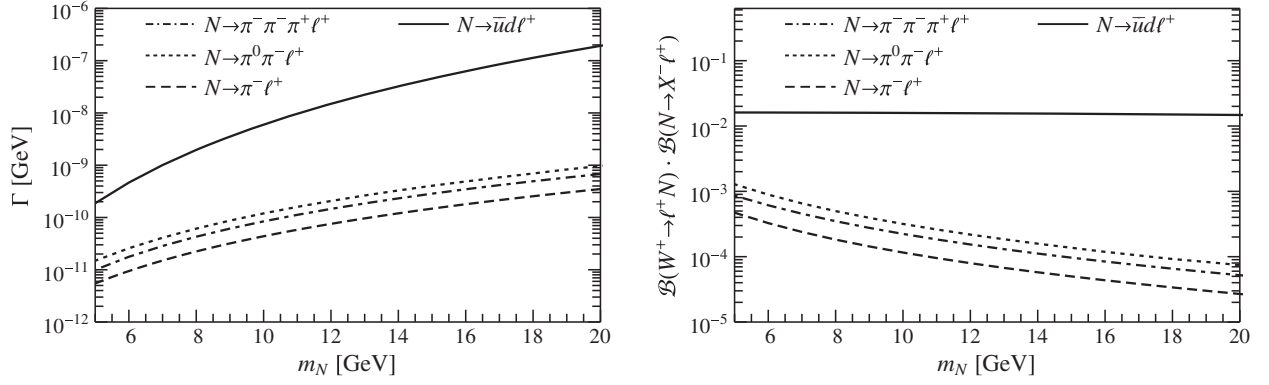
FIG. 1. Canonical decay rates for $N \to \pi^- \ell^+$, $N \to \pi^0 \pi^- \ell^+$, $N \to \pi^- \pi^- \pi^+ \ell^+$, and the inclusive mode $N \to \bar{u} d \ell^+$ (left) and canonical branching ratios for the full processes $W^+ \to \ell^+ \ell^+ n\pi$ (right) as a function of the neutrino mass m_N, with all mixing factors $|U_{\ell N}|$ removed. To obtain the actual values, the canonical values must be multiplied by the factor $|U_{\ell N}|^2$ (left), or $|U_{\ell N}|^4 / \sum_{l_i} |U_{\ell_i N}|^2$ (right).

One last important point in the observability of these processes is the long lifetime of N, which would cause an observable displacement in the detector between the production and decay vertices of N. This displacement will drastically help reduce the possible backgrounds. For a sterile neutrino N with a mass in the range 5–20 GeV, the total width can be estimated as [23,38]

$$\Gamma_N \sim \frac{G_F^2 m_N^5}{12\pi^3} \sum_\ell |U_{\ell N}|^2. \qquad (7)$$

This expression disregards hadronization effects in the final state; to include hadronization, more detailed calculations [53] change this result by about 12% in our mass range of interest. The lighter N and the smaller the mixing $|U_{\ell N}|^2$ are, the longer N will live. Using the current upper bound $|U_{\ell N}|^2 \sim 10^{-5}$, the characteristic displacement $\tau c \equiv \hbar c / \Gamma_N$ is in the range $\sim 20\ \mu m$ to 20 mm (for 20 and 5 GeV, respectively). For smaller $|U_{\ell N}|^2$, the displacements will be proportionally larger. Moreover, the relativistic γ factor will increase the displacement as well.

III. DETECTOR SIMULATIONS AND DISCUSSION

Now we run simulations in order to study the observability of these modes at the LHC. In principle, they could be observed provided the pions can be identified and the background can be reduced using the spatial displacement
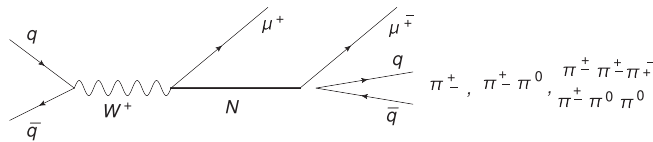

FIG. 2. Heavy neutrino produced via charged current Drell-Yan process: $pp \to W^+ \to \mu^+ N(\to \mu^\mp + n\pi)$. The second muon as μ^+ corresponds to a Majorana N; for μ^-, it corresponds to either a Dirac or Majorana N.

between the production and decay vertices of the heavy neutrino N. This vertex displacement should be observable for m_N below 20 GeV [29,30].

We simulated the whole process shown in Fig. 2, namely, $pp \to W \to \mu N, N \to \mu + n\pi$ at 13 TeV center-of mass energy, generating a sample of 15000 $W \to \mu N$ events. We use MADGRAPH5_AMC@NLO [54] to generate heavy neutrinos via the charge current Drell-Yan process shown in Fig. 2. Then, decay and hadronization processes are done with PYTHIA 8.1 [55,56]. A fast detector simulation is performed by DELPHES 3 [57]; we use the card ATLAS.tcl included in the package. The Universal FeynRules Output [58] files were implemented with Wolfram *Mathematica* [59] using the FeynRules libraries [60].

As a trigger, we use events with two muons: one with $p_T > 10$ GeV and the other with $p_T > 4$ GeV. Concerning the W and N reconstruction, the events are selected based on the ATLAS/CMS [61,62] standard requirements: muon $p_T > 10$ GeV, $|\eta| < 2.5$, and tracks $p_T > 500$ MeV and $|\eta| < 2.5$. As the heavy-neutrino mass is considered to be smaller than 20 [GeV], the quarks produced in the neutrino decay are likely to hadronize in the specific pion states described above. We also require events with at least two muons where one of them must show a transverse momentum significantly larger than the other (see Table I).

The two muons plus the pions coming from the N decay should reconstruct the W mass. In addition, the less energetic muon plus the pions should reconstruct the N mass. However, we must take into account that the neutral pions in the final state will not be detected: They decay immediately into two almost collinear photons which will

TABLE I. Cuts used for the event selection and reconstruction.

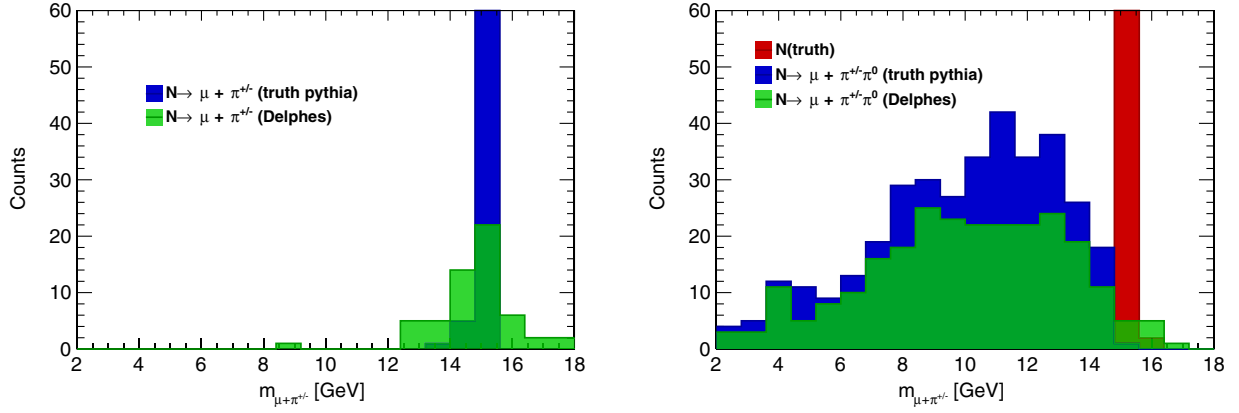|	Prompt μ	Displaced μ	Displaced tracks (pions)
p_T	>10 GeV	>4 GeV	>0.5 GeV
$|\eta|$	<2.5	<2.5	<2.5

FIG. 3.   Simulation of a heavy neutrino reconstructed in hypothetically isolated processes $N \rightarrow \mu^{\pm}\pi^{\mp}$ (left) and $N \rightarrow \mu^{\pm}\pi^{\mp}\pi^{0}$ (right) where the π^{0} cannot be detected. In both cases, the invariant mass is of the pair muon-charged pion. Red: Idealized case where all particles including neutral pions are detected. Blue: Simulation where neutral pions are not detected. Green: The same as blue but smeared by detector resolution (DELPHES). A sample of 15000 events $W \rightarrow \mu N$ was used, with a benchmark $m_N = 15$ GeV.

not have enough energy to be distinguished from noise in the EM calorimeter in the cases of interest $m_N < 20$ GeV. Therefore, we can have only two types of events: (i) the muons and one charged pion and (ii) the muons and three charged pions. The latter corresponds clearly to $N \rightarrow \mu^{\pm}\pi^{\pm}\pi^{\mp}\pi^{\mp}$, but the former will be the sum of the three decay modes, namely, $N \rightarrow \mu^{\pm}\pi^{\mp}$, $N \rightarrow \mu^{\pm}\pi^{\mp}\pi^{0}$, and $N \rightarrow \mu^{\pm}\pi^{\mp}\pi^{0}\pi^{0}$.

In Fig. 3 (left), we show the simulation of the hypothetical case in which the decay into a single pion, $N \rightarrow \mu^{\pm}\pi^{\mp}$, could be separated from the decays $N \rightarrow \mu^{\pm}\pi^{\mp}\pi^{0}, \mu^{\pm}\pi^{\mp}\pi^{0}\pi^{0}$ (this separation is not realistic, because neutral pions are not detected). The peak at m_N is clear. In Fig. 3 (right), we simulate the decay into two pions, where one of the pions has to be neutral due to charge conservation: $N \rightarrow \mu^{\pm}\pi^{\mp}\pi^{0}$. Now, since the π^{0} is not observed, the distribution shows that effect as an extended continuum into lower invariant masses, with an upper cutoff at m_N.

In Fig. 4, we show the simulations for the decay into three pions. Now there are two modes: $\mu^{\pm}\pi^{\mp}\pi^{0}\pi^{0}$ (left) and $\mu^{\pm}\pi^{\pm}\pi^{\mp}\pi^{\mp}$ (right). In Fig. 4 (left), one can see again a continuous distribution due to the missing $\pi^{0}\pi^{0}$, which is even more pronounced to low invariant masses of the charged pair, compared to the single missing π^{0} of Fig. 3 (left). In contrast, the three-charged pion mode shows in Fig. 4 (right) shows a clear reconstruction of the peak at m_N.

In a realistic case, therefore, the search for a mode with a single charged pion will be the sum of the three pionic final states $\pi^{\pm}$, $\pi^{\pm}\pi^{0}$, and $\pi^{\pm}\pi^{0}\pi^{0}$, as we show in the simulations in Fig. 5 (there are modes with even more pions, but those are suppressed with respect to the three cases considered here). Figure 5 (left) shows the result from PYTHIA and Fig. 5 (right) the smeared distribution due to detector resolution given by DELPHES. The latter is a more spread distribution, but qualitatively they are similar in the sense
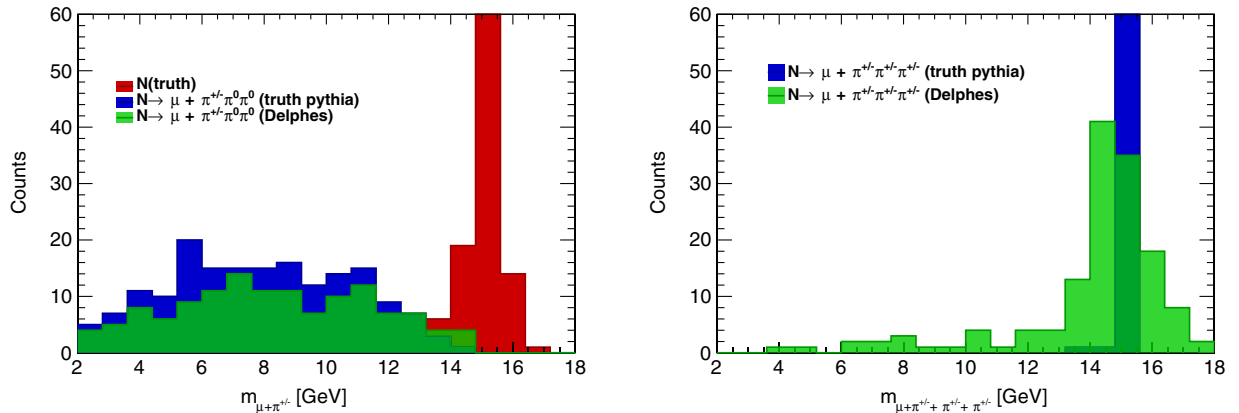

FIG. 4.   Simulation of a heavy neutrino reconstructed in hypothetically isolated process $N \rightarrow \mu^{\pm}\pi^{\mp}\pi^{0}\pi^{0}$ (left) and in the three-charged pion mode $N \rightarrow \mu^{\pm}\pi^{\pm}\pi^{\mp}\pi^{\mp}$. Red: Idealized case where all particles including neutral pions are detected. Blue: Simulation where neutral pions are not detected. Green: The same as red but smeared by detector resolution. A sample of 15000 events $W \rightarrow \mu N$ was used, with a benchmark $m_N = 15$ GeV.
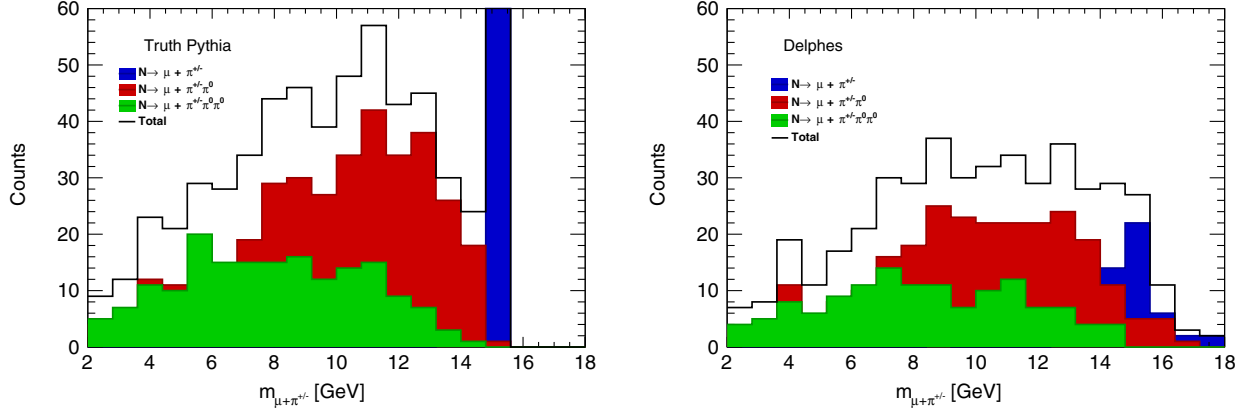
FIG. 5. Simulation of a heavy neutrino reconstructed in events with a muon and a single charged pion. The events combine the decays into $\mu^{\pm}\pi^{\mp}$, $\mu^{\pm}\pi^{\mp}\pi^0$, and $\mu^{\pm}\pi^{\mp}\pi^0\pi^0$ where the neutral pions are missing. A sample of 15000 events $W \rightarrow \mu N$ was used, with a benchmark $m_N = 15$ GeV.

that the dominant feature is a continuous distribution with an upper end point at the N mass. The single-pion decay channel with no neutral pions, namely, $N \rightarrow \mu^{\pm}\pi^{\mp}$, which is the only mode with a clear peak, is suppressed compared to the other two channels, and its peaked feature is lost in the distribution. This feature contrasts with the events with three charged pions, shown in Fig. 4 (right), where the peak is still clear. In a real search, there should be a continuous part due to the four-pion mode, but it is subdominant.

Besides the reconstruction of the N, one should verify the reconstruction of the W from the full event, which essentially adds the prompt muon to the decay of N. Given that we are considering $m_N < 20$ GeV, i.e., considerably lighter than M_W, the prompt muon should be more energetic that the one coming for the N decay, and, due to the relatively long lifetime of an N with such masses, the decay vertex of N should be displaced with respect to the prompt muon. Figure 6 shows the distributions for the W reconstruction in the respective modes for the N decays described above, namely, with a single charged pion (left) and in the mode with three charged pions (right).

Concerning the reconstruction efficiencies at the LHC for our particles of interest, these constitute no major limitation in the results, since for muons it is above 98% [63], while for pions the tracking efficiency is near 90% [64,65]. For the displaced vertex efficiency, one should expect near 50% for four charged tracks [66], although we did not require vertex displacement in the analysis to build Figs. 3–6. As stated at the end of Sec. II, the characteristic displacement due to the long N lifetime could be from a few tens of micrometers to a few meters, depending on m_N and the mixing. This implies that a fraction of the decays occur outside the range of observability of the detector. If we consider a minimum and maximum observable displacement, L_0 and L_1, respectively, the acceptance factor (the probability that the decay occurs within the fiducial volume of the detector) will be

$$ac = (e^{-\gamma L_0/\tau c} - e^{-\gamma L_1/\tau c}). \qquad (8)$$

The efficiency and acceptance factors should be determined by the specific experiment using the data and detector, so we did not include them in the previous analysis.
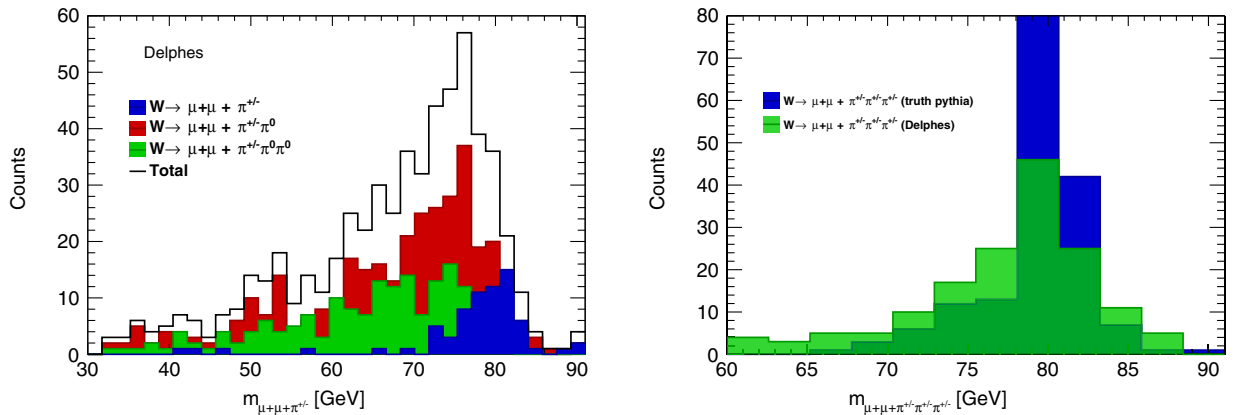

FIG. 6. Simulation of the W boson decaying into μN followed by the N decay, reconstructed in events with two muons and a single charged pion (left) and three charged pions (right). A sample of 15000 events $W \rightarrow \mu N$ was used, with a benchmark $m_N = 15$ GeV.
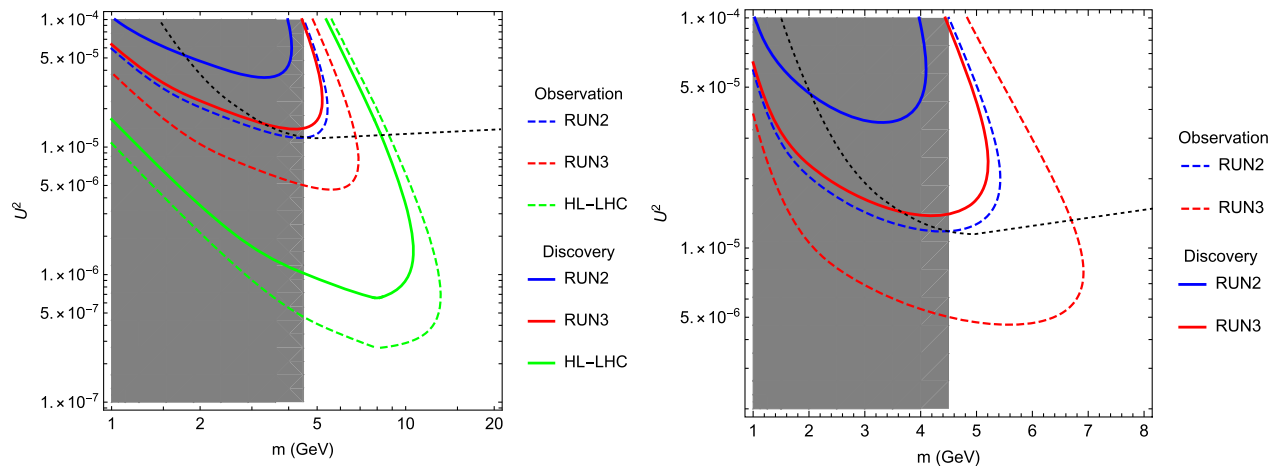
FIG. 7. Sensitivity of $pp \to \mu N(N \to n\pi\mu)$ to the mixing $|U_{\mu N}|^2$, as a function of the sterile neutrino mass m_N, for LHC run 2 (150 fb^{-1}), run 3 (300 fb^{-1}), and the High-Luminosity LHC (3000 fb^{-1}). A vertex displacement detectability between 1 mm and 30 cm is assumed. The dashed curves correspond to four events for observation and the solid curves to nine events for discovery. The black dotted line is the current bound from DELPHI [68]. The gray region is affected by backgrounds not considered in the analysis, and so the limits are less reliable there.

Nevertheless, in order to have an estimate of the potential sensitivity of these pionic modes to the neutrino mixing $|U_{\mu N}|^2$, we have simulated the events for assumed values $L_0 = 1$ mm and $L_1 = 30$ cm. The sensitivity curves for LHC run 2, LHC run 3, and the LH-LHC are shown in Fig. 7. The curves show the smallest values of $|U_{\mu N}|^2$ to observe four events (dashed lines) or nine events (solid lines), which would correspond to 3σ and 5σ, respectively, assuming one background event [67]. The current limit by DELPHI [68] is also shown.

The sensitivity curves also include the cuts in Table I, a 50% efficiency factor for muon, tracking, and displaced vertex (DV) detection, the DV acceptance factor of Eq. (8) with the assumed values of L_0 and L_1 associated to the detector, and the average value of the relativistic factor γ for each given mass. The curves would extend to lower m_N values if the detector length L_1 is larger than the assumed value of 30 cm and would extend to larger m_N values if the smallest observable displacement L_0 is smaller than the assumed value of 1 mm.

From Fig. 7, one can see that run 2 does not seem to improve on the current bound imposed by DELPHI, while run 3 has a potential to tighten the bound on the mixing by an order of magnitude for m_N in the low-mass range (around 5–7 GeV). In contrast, the High-Luminosity LHC (HL-LHC) could improve the bounds by about 2 orders of magnitude in the mass range below 11 GeV.

The figures above are obtained from simulations of the signal only. In order to eliminate backgrounds in the actual experiment, one should also request (a) a minimal amount of missing E_T—with this cut, one would remove all events that have SM neutrinos, such as W^+W^- or $t\bar{t}$ production; (b) a displaced vertex associated with the muon with lower p_T—as stated before, for $m_N < 20$ GeV the prompt muon

is more energetic than the second muon, and the latter should come from a displaced secondary vertex, because the decaying N is rather long living. This cut should remove almost all remaining backgrounds with the exception of heavy flavors, e.g., B hadrons, that typically decay into one displaced muon plus tracks; and (c) isolation in the prompt muon in addition to the requirement that the invariant mass of the two muons plus the tracks should be close to the W mass.

In general, the background-free hypothesis with displaced vertices can be trusted only for masses larger than about 5 GeV, where no N is produced from meson decays. Consequently, Fig. 7 appears in gray for masses below 4.5 GeV. For masses below this boundary, one can largely reject backgrounds using cuts (a)–(c), because all mesons that may lead to displaced vertices are most of the time produced within jet fragments. In particular, cut (c), i.e., "muon isolation," should remove largely those backgrounds and remove even more by adding the cut of W invariant mass of the full system. One may expect that no SM background should remain after cuts (a)–(c), but to quantify this statement is an issue that goes beyond this work. Concerning backgrounds due to nuclear interactions with the detector material [33], these are largely suppressed by the requirement of having one muon be part of the displaced vertex reconstruction.

IV. CONCLUSIONS

In this work, we have studied the observability at the LHC of the exclusive process $W \to \mu N(\to \mu + n\pi)$, which is appropriate to discover a sterile neutrino N with a mass in the range 5 GeV $< m_N <$ 20 GeV. This is an intermediate region where neither rare meson decays (B, D, etc.) nor $pp \to \ell\ell jj, \ell\ell\ell\nu$ modes at the LHC are sensitive to the

presence of such neutrinos. The modes we use are exclusive semileptonic, containing pions in their hadronic component. Because of the pions in the final state, the reconstruction of the events at a hadron collider is not a trivial matter. However, one particular feature of this process that helps reducing drastically all backgrounds is the fact that a sterile neutrino N with a mass below 20 GeV should have a lifetime long enough to travel an observable distance in the detector before it decays. Indeed, given the current upper bounds on the sterile neutrino mixing with the muon flavor $|U_{\mu N}|^2 \lesssim 10^{-5}$, a vertex displacement above 20 μm would occur for $m_N = 20$ GeV and longer than 20 mm for $m_N = 5$ GeV.

Naïvely, the most favorable mode should have a single charged pion in the final state, namely, $N \to \mu^{\pm} \pi^{\mp}$. However, this mode is suppressed compared to the two-pion and three-pion modes. Moreover, since neutral pions would go undetected at the LHC, the single charged pion events will contain the modes $N \to \mu^{\pm} \pi^{\mp} \pi^0$ and $N \to \mu^{\pm} \pi^{\mp} \pi^0 \pi^0$ as well. We have simulated the events that contain one prompt muon, followed by a displaced muon and charged pion (the second muon should also have less p_T than the prompt muon). The invariant mass of the displaced charged particles $\mu^{\pm} \pi^{\mp}$ will show a continuous distribution with an upper end point at the N mass, and the invariant mass of all three charged particles $\mu\mu\pi$ will show a continuous distribution with an end point at M_W.

Accordingly, the cleanest mode is the one with three charged pions in the final state: $N \to \mu^{\pm} \pi^{\pm} \pi^{\mp} \pi^{\mp}$. Modes with more pions are suppressed compared to this one, so we have neglected their effect in the invariant mass distributions (one would expect only a small continuous tail to lower invariant masses, due to the modes with additional neutral pions that go undetected). In this mode, the invariant mass of the secondary muon and the charged pions will show a peak at m_N, and the invariant mass that includes the prompt muon will show a peak at M_W.

These exclusive semileptonic processes with their feature of vertex displacement can improve the current upper bounds on the mixing of sterile neutrinos with the muon flavor. LHC run 3 can improve the bound by an order of magnitude for m_N only in the lower end (5–7 GeV), while an improvement about 2 orders of magnitude in the bound can be achieved with the High-Luminosity LHC for m_N below 11 GeV, where our proposed semileptonic modes are advantageous over other processes. For masses above 11 GeV, these semileptonic modes do not seem to give an improvement in the bound, unless the detector is able to distinguish vertex displacements shorter than 1 mm as was assumed in these simulations.

ACKNOWLEDGMENTS

[1] Y. Fukuda *et al.* (Super-Kamiokande Collaboration), Phys. Rev. Lett. **81**, 1562 (1998).

[2] Q. R. Ahmad *et al.* (SNO Collaboration), Phys. Rev. Lett. **89**, 011301 (2002).

[3] K. Eguchi *et al.* (KamLAND Collaboration), Phys. Rev. Lett. **90**, 021802 (2003).

[4] M. C. Gonzalez-Garcia and M. Maltoni, Phys. Rep. **460**, 1 (2008).

[5] R. N. Mohapatra and A. Y. Smirnov, Annu. Rev. Nucl. Part. Sci. **56**, 569 (2006).

[6] V. Barger, D. Marfatia, and K. Whisnant, Int. J. Mod. Phys. E **12**, 569 (2003).

[7] A. Strumia and F. Vissani, arXiv:hep-ph/0606054.

[8] P. Minkowski, Phys. Lett. **67B**, 421 (1977).

[9] T. Yanagida, Conf. Proc., **C7902131**, 95 (1979).

[10] P. Ramond, in *Proceedings of the International Symposium on Fundamentals of Quantum Theory and Quantum Field Theory, Palm Coast, Florida* (1979), pp. 265–280, https://arxiv.org/abs/hep-ph/9809459.

[11] M. Gell-Mann, P. Ramond, and R. Slansky, Conf. Proc., **C790927**, 315 (1979).

[12] S. L. Glashow, NATO Sci. Ser. B **61**, 687 (1980).

[13] R. N. Mohapatra and G. Senjanovic, Phys. Rev. Lett. **44**, 912 (1980).

[14] J. Schechter and J. W. F. Valle, Phys. Rev. D **25**, 774 (1982).

[15] F. F. Deppisch, P. S. B. Dev, and A. Pilaftsis, New J. Phys. **17**, 075019 (2015).

[16] S. Chatrchyan *et al.* (CMS Collaboration), Phys. Lett. B **717**, 109 (2012).

[17] G. Aad *et al.* (ATLAS Collaboration), J. High Energy Phys. 07 (2015) 162.

[18] W.-Y. Keung and G. Senjanovic, Phys. Rev. Lett. **50**, 1427 (1983).

[19] F. del Aguila, J. A. Aguilar-Saavedra, and R. Pittau, J. High Energy Phys. 10 (2007) 047.

[20] A. Atre, T. Han, S. Pascoli, and B. Zhang, J. High Energy Phys. 05 (2009) 030.

[21] A. Das, P. Konar, and A. Thalapillil, J. High Energy Phys. 02 (2018) 083.

[22] G. Cvetic, C. Dib, and C. S. Kim, J. High Energy Phys. 06 (2012) 149.

[23] C. O. Dib and C. S. Kim, Phys. Rev. D **92**, 093009 (2015).

[24] E. Izaguirre and B. Shuve, Phys. Rev. D **91**, 093010 (2015).

[25] C. O. Dib, C. S. Kim, K. Wang, and J. Zhang, Phys. Rev. D **94**, 013005 (2016).

[26] C. O. Dib, C. S. Kim, and K. Wang, Chin. Phys. C **41**, 103103 (2017).

[27] C. O. Dib, C. S. Kim, and K. Wang, Phys. Rev. D **95**, 115020 (2017).

[28] S. Dube, D. Gadkari, and A. M. Thalapillil, Phys. Rev. D **96**, 055031 (2017).

[29] J. C. Helo, M. Hirsch, and S. Kovalenko, Phys. Rev. D **89**, 073005 (2014); **93**, 099902(E) (2016).

[30] C. Dib and C. S. Kim, Phys. Rev. D **89**, 077301 (2014).

[31] A. M. Gago, P. Hernandez, J. Jones-Perez, M. Losada, and A. Moreno Briceño, Eur. Phys. J. C **75**, 470 (2015).

[32] S. Antusch, E. Cazzato, and O. Fischer, Phys. Lett. B **774**, 114 (2017).

[33] G. Cottin, J. C. Helo, and M. Hirsch, Phys. Rev. D **97**, 055025 (2018).

[34] M. Nemevsek, F. Nesti, and G. Popara, Phys. Rev. D **97**, 115018 (2018).

[35] G. Cottin, J. High Energy Phys. 03 (2018) 137.

[36] A. Abada, N. Bernal, M. Losada, and X. Marcano, J. High Energy Phys. 01 (2019) 093.

[37] I. Boiarska, K. Bondarenko, A. Boyarsky, S. Eijima, M. Ovchynnikov, O. Ruchayskiy, and I. Timiryasov, arXiv:1902.04535.

[38] M. Drewes and J. Hajer, arXiv:1903.06100.

[39] C. O. Dib, C. S. Kim, N. A. Neill, and X.-B. Yuan, Phys. Rev. D **97**, 035022 (2018).

[40] G. Cvetic, C. Dib, S. K. Kang, and C. S. Kim, Phys. Rev. D **82**, 053010 (2010).

[41] R. Aaij et al. (LHCb Collaboration), Phys. Rev. D **85**, 112004 (2012).

[42] G. Cvetic and C. S. Kim, Phys. Rev. D **96**, 035025 (2017).

[43] C. Dib, V. Gribanov, S. Kovalenko, and I. Schmidt, Phys. Lett. B **493**, 82 (2000).

[44] C. S. Kim, G. Lopez Castro, and D. Sahoo, Phys. Rev. D **96**, 075016 (2017).

[45] C. Patrignani et al. (Particle Data Group), Chin. Phys. C **40**, 100001 (2016).

[46] V. Cirigliano, G. Ecker, and H. Neufeld, Phys. Lett. B **513**, 361 (2001).

[47] V. Cirigliano, G. Ecker, and H. Neufeld, J. High Energy Phys. 08 (2002) 002.

[48] M. Fujikawa et al. (Belle Collaboration), Phys. Rev. D **78**, 072006 (2008).

[49] J. P. Lees et al. (BABAR Collaboration), Phys. Rev. D **86**, 032013 (2012).

[50] S. J. Brodsky, G. F. de Teramond, H. G. Dosch, and J. Erlich, Phys. Rep. **584**, 1 (2015).

[51] D. Gómez Dumm, P. Roig, A. Pich, and J. Portolés, Phys. Rev. D **81**, 034031 (2010).

[52] G. Aad et al. (ATLAS Collaboration), Phys. Lett. B **759**, 601 (2016).

[53] K. Bondarenko, A. Boyarsky, D. Gorbunov, and O. Ruchayskiy, J. High Energy Phys. 11 (2018) 032.

[54] J. Alwall, R. Frederix, S. Frixione, V. Hirschi, F. Maltoni, O. Mattelaer, H. S. Shao, T. Stelzer, P. Torrielli, and M. Zaro, J. High Energy Phys. 07 (2014) 079.

[55] T. Sjostrand, S. Mrenna, and P. Z. Skands, Comput. Phys. Commun. **178**, 852 (2008).

[56] T. Sjostrand, S. Mrenna, and P. Z. Skands, J. High Energy Phys. 05 (2006) 026.

[57] J. de Favereau, C. Delaere, P. Demin, A. Giammanco, V. Lemaitre, A. Mertens, and M. Selvaggi (DELPHES 3 Collaboration), J. High Energy Phys. 02 (2014) 057.

[58] C. Degrande, C. Duhr, B. Fuks, D. Grellscheid, O. Mattelaer, and T. Reiter, Comput. Phys. Commun. **183**, 1201 (2012).

[59] Wolfram Research, Inc., Mathematica, Version 11.3 (Wolfram Research, Inc., Champaign, IL, 2018).

[60] A. Alloul, N. D. Christensen, C. Degrande, C. Duhr, and B. Fuks, Comput. Phys. Commun. **185**, 2250 (2014).

[61] G. Aad et al. (ATLAS Collaboration), J. Instrum. **3**, S08003 (2008).

[62] S. Chatrchyan et al. (CMS Collaboration), J. Instrum. **3**, S08004 (2008).

[63] G. Aad et al. (ATLAS Collaboration), Eur. Phys. J. C **76**, 292 (2016).

[64] M. Aaboud et al. (ATLAS Collaboration), Eur. Phys. J. C **77**, 673 (2017).

[65] Early inner detector tracking performance in the 2015 data at $\sqrt{s} = 13$ TeV, ATLAS Collaboration Technical Report No. ATL-PHYS-PUB-2015-051, 2015.

[66] Performance of vertex reconstruction algorithms for detection of new long-lived particle decays within the ATLAS inner detector, Technical Report No. ATL-PHYS-PUB-2019-013, 2019.

[67] G. Cowan, K. Cranmer, E. Gross, and O. Vitells, Eur. Phys. J. C **71**, 1554 (2011); **73**, 2501(E) (2013).

[68] P. Abreu et al. (DELPHI Collaboration), Z. Phys. C **74**, 57 (1997); **75**, 580(E) (1997).